A unified photocatalytic strategy for the cross coupling of alcohols with aryl halides enabled by synergistic nickel and iron LMCT catalysis

Mohammad Jaber,[†] Yasemin Ozbay,[†] Gaël Tran,*[†] and Abderrahmane Amgoune*[,†,§]

† Université Lyon 1, Institut de Chimie et Biochimie Moléculaires et Supramoléculaires (ICBMS, UMR 5246 du CNRS), 1 rue Victor Grignard, 69100 Villeurbanne, France.

§ Institut Universitaire de France (IUF), 1 rue Descartes, 75231 Paris, France.

KEYWORDS: Nickel catalysis – Iron catalysis – Native alcohols – Cross-coupling – Mechanistic study

ABSTRACT: The use of alcohol feedstock as coupling partner in cross coupling reactions offers an extraordinary potential for the efficient synthesis of Csp^3-rich complex molecular scaffolds. This prominent strategy relies on the generation of alkoxy radicals, which can react *via* various radical pathways to give carbon-centered radicals that can be engaged in C–C bond formation reactions. However, cross-coupling reactions involving catalytic generation of alkoxy radicals directly from native alcohols is highly challenging and the scope of existing catalytic methods remains particularly limited. Moreover, a unified strategy that can incorporate a broad range of alcohols in catalytic cross-coupling with aryl halides is currently unavailable. Herein, we report a general photocatalytic platform that combines nickel and iron ligand-to-metal charge transfer (LMCT) catalysis for the selective deconstructive Csp^2-Csp^3 bond cleavage and arylation of various unactivated alcohols. This protocol leverages the ability of photoinduced iron LMCT catalysis to generate radicals from diversely substituted alcohols, enabling implementation of various C–C bond-forming manifolds. These include dehydroxymethylative arylation of aliphatic alcohols, remote arylation of cyclic alcohols to yield alkyl ketones, and unprecedented use of tertiary alcohols for methylation of aryl halides. This methodology offers a practical and unified strategy for engaging a large variety of commercially available alcohols in cross-coupling reactions under mild conditions, using abundant nickel and iron catalysts. Mechanistic studies, including stoichiometric organometallic chemistry and cyclic voltammetry, provide unprecedented insights into the crucial role of the ancillary ligand surrounding the iron catalyst in stabilizing high-valent photo-catalytically active intermediates.

1. Introduction

Bioactive compounds containing a high amount of Csp^3 centers tend to feature highly improved properties compared to more saturated analogues, *e.g.* better solubility profile or fewer off-target effects, resulting in improved pharmaco-kinetic and -dynamic profiles.[1] Recognizing this trend, the organic chemistry community has rapidly developed novel synthetic routes to sp^3-rich compounds. In particular, the renaissance of cross-couplings using first-row transition metal catalysts and the subsequent rise of metallaphotoredox catalysis have led to some of the most impactful methods in this field.[2] This radical-based approach has been so successful that a wide range of carbon radical precursors have been explored, including alkyl halides, silicates, trifluoroborates, carboxylates, redox-active esters or Katrizky salts.[3]

While these precursors cover significant chemical space, most are not "*native*" chemicals, reflected in their relatively low commercial availability and often cumbersome synthesis. In contrast, alcohols are ubiquitous both in natural and commercial sources and exhibit exceptional structural diversity, making them highly attractive as carbon-based radical precursors for cross-coupling reactions.[4] However, converting alcohols into carbon-based radicals is notoriously difficult, *typically requiring pre-activation of the alcohol* followed by homolytic cleavage of the resulting intermediate.[5] Although generally straightforward, these methods generate unnecessary waste, reducing the overall sustainability of the reaction and often limiting applicability to specific classes of alcohols.

Recent advances in modern photoredox strategies have enabled the catalytic generation of carbon-based radicals from free alcohols under mild conditions.[6] These photocatalytic strategies mainly rely on the photocatalytic formation of an alkoxy radical from the alcohol either via proton-coupled electron transfer (PCET) or ligand-to-metal charge transfer (LMCT), followed by transposition to carbon-based radical (Scheme 1A).

Despite these breakthroughs, the catalytic transformation of free alcohols into carbon-based radicals remains extremely rare within the context of metallaphotoredox catalysis, with only two notable examples to date. The group of Rueping achieved arylative ring opening reactions from cyclic alkanols bearing electron-rich aromatic cores by combining PCET catalysis with nickel catalysis.[7] Meanwhile, the group of Zuo employed a LMCT process from cerium complexes, resulting in photocatalytic dehydroxymethylative arylation of primary aliphatic alcohols.[8] These elegant examples highlight the synthetic versatility offered by alkoxy radicals, as

cycloalkanols lead to arylated ketones through C–C bond functionalization, whereas linear alcohols result in arylated alkyls through dehydroxymethylation. However, these protocols are limited to specific classes of alcohols. PCET activation is inherently restricted to oxidizable substrates, while LMCT from cerium complexes does not accommodate sterically hindered alcohols in this context. Considering the tremendous synthetic potential offered by implementing alkoxy radicals in nickel catalyzed radical cross-coupling reactions, we aimed to develop a general catalytic platform capable of coupling a broad range of alcohols.

Achieving generality in metallaphotoredox catalysis is particularly challenging, as the intricate catalytic cycles must be kinetically matched to prevent the accumulation and degradation of catalytic intermediates. In this perspective, we aimed to explore the photoinduced LMCT excitation strategy for several reasons: (*i*) LMCT catalysts are based on abundant and inexpensive transition metals such as copper, cerium, or iron, (*ii*) these catalysts operate through distinct photochemical pathways compared to commonly used photoredox catalysts. While the domain of photoredox catalysis is largely dominated by photocatalysts operating via outer-sphere single electron transfer processes, LMCT catalysts function through inner-sphere pathways.[9] Specifically, transition metals with LMCT excited states commonly undergo visible light-induced homolysis.[10] This mode of reactivity enables the transformation of nucleophilic entities into open shell species *via* inner-sphere process involving coordination of the substrate to the metal center, followed by photoinduced bond homolysis to generate a formally reduced metal center and a radical. This activation mode, proceeding through coordination chemistry, offers extensive opportunities to fine-tune the steric and electronic parameters governing the alcohol coordination and alkoxy radical generation steps. With these considerations in mind, we hypothesized that an effective LMCT catalyst should possess a low coordination number, allowing for the indiscriminate coordination of various types of alcohols. This feature would ensure continuous kinetic matching between catalytic cycles, even when the substrate classes change. We identified iron complexes as particularly promising due to their reported photoactivity in less crowded conformations.[11,12]

Herein we report a unified and practical photocatalytic strategy that enable various type of cross-coupling manifolds with primary and tertiary alcohols. These include: *(i)* dehydroxymethylative arylation of aliphatic alcohols, *(ii)* remote arylation of cyclic alcohols to yield alkyl ketones, and *(iii)* the unprecedented use of tertiary alcohols as methyl radical source for the methylation of aryl halides. The photocatalytic platform comprises a photoactive iron-LMCT catalyst capable of generating alkoxy radicals from a broad range of alcohols, and a nickel catalyst that promotes the oxidative addition of the aryl halide electrophilic partner, the capture of the alkyl radical and C–C bond formation. Catalytic turnover for both cycles is insured by an organophotoredox catalyst that acts as a redox shuttle between the two catalytic cycles.

Mechanistic investigations have validated the role of each catalytic partner and provided key insights into the crucial role of the ancillary ligand surrounding the iron catalyst, which is essential for the efficient conversion of a broad range of alcohols.

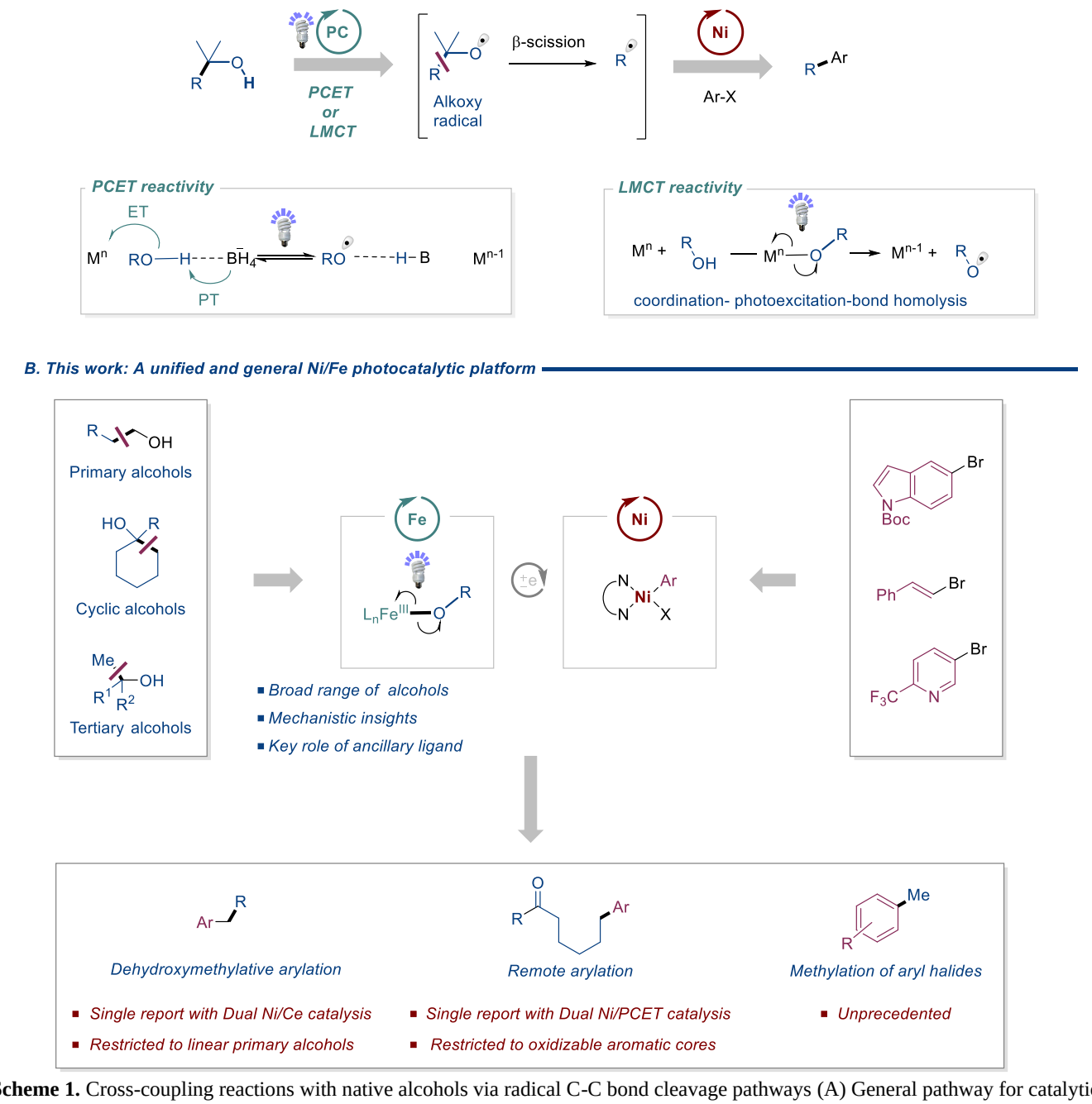

Scheme 1. Cross-coupling reactions with native alcohols via radical C-C bond cleavage pathways (A) General pathway for catalytic transposition of alcohols to carbon-based radicalvia the PCET or LMCT strategy. (B) This work: A general protocol allowing the valorization of a broad range of alcohols.

2. Results and discussion

2.1. Optimization

Aryl bromide **1a** and alcohol **2a** were chosen as model substrates and engaged in the cross-coupling using $FeCl_3$ as the LMCT catalyst, $NiCl_2$.DME/dMeBpy(**L**$_{Ni1}$) as the cross-coupling catalyst, 1,10-diphenylanthracene (DPA) as electron shuttle between the [Fe] and the [Ni] cycle, Na_3PO_4 as a base, in MeCN and under 390 nm irradiation (Scheme 2). Disappointingly, alcohol activation appeared to be inefficient in these conditions as only traces of product were formed. Since the iron coordination sphere is known to have a large impact on the efficiency of [Fe^{III}] LMCT systems,[13] we decided to focus our attention on anionic ligands. While simple halides did not prove efficient (<5% yield), aryl carboxylates (formed *in-situ* from the corresponding free acids) appeared to significantly increase the yield (Scheme 2A), leading to 30% yield in the case of simple benzoic acid **L**$_{Fe1}$. A range of carboxylic acids featuring

various stereoelectronic profiles were investigated, eventually leading to the selection of the sterically hindered carboxylate $\mathbf{L_{Fe9}}$ (70% yield). The other reaction parameters were also systematically investigated, although none of them appeared to be as impactful as the iron ligand (see SI for full tables). Ultimately, the combination of $FeCl_2$ (10 mol%), $\mathbf{L_{Fe9}}$ (35 mol%), $NiCl_2$.DME (2.5 mol%), $\mathbf{L_{Ni8}}$ (2.5 mol%), DPA (2.5 mol%) and K_3PO_4 (3.0 eq) in MeCN under 390 nm irradiation led to 85% yield of **3a** (78% isolated).

Scheme 2. Ni/Fe catalyzed arylation of linear alcohols: selected optimization experiments.

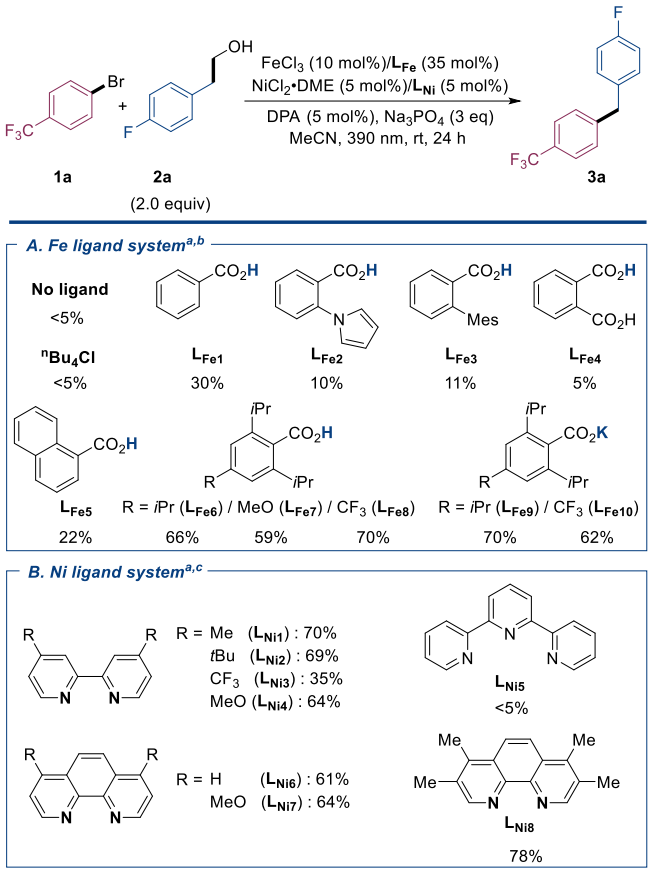

[a] Reactions performed on 0.20 mmol scale. Yields were determined by ^{19}F NMR using $PhOCF_3$ as an internal standard. [b] $\mathbf{L_{Ni}} = \mathbf{L_{Ni1}}$. [c] $\mathbf{L_{Fe}} = \mathbf{L_{Fe9}}$.

In addition to efficiently activating primary alcohols, we were pleased to see that this catalytic system was also suitable for the cross-coupling of much more sterically hindered tertiary cycloalkanols (Scheme 3). By contrast, cerium LMCT catalyst was unable to yield any trace of **23** under the same conditions, thus giving credit to our initial hypothesis on the critical role of the LMCT catalyst's coordination number.

Scheme 3. Catalytic system efficient with sterically hindered alcohols.

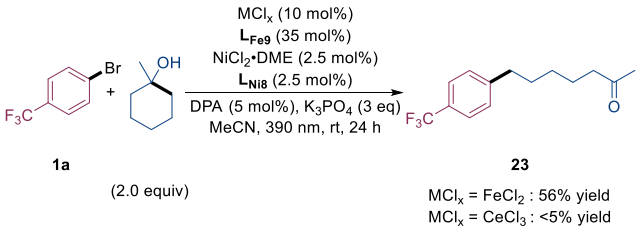

2.2. Scope and limitations

With the optimized conditions in hand, the scope of this reaction was investigated with a range of aryl bromides **1** and primary alcohols **2** (Scheme 4). Pleasingly, the reaction appeared to be largely insensitive to the electronic parameters of the aryl bromide partner **1**, with yields ranging from 59% to 88% (**3-10**) regardless of the electron-rich or electron-poor nature of the aryl ring. Sensitive functionalities such as a cyano group (**4**, 88%) or a chlorine atom (**5**, 56%) were well tolerated. Significantly, biologically relevant heteroaryl bromides were compatible in the reaction (**11-14**), including strongly coordinating unsubstituted pyridine (**12**, 50% yield) and pyrimidine (**13**, 70%). Apart from aryl bromides, a vinyl bromide was also engaged and led to the desired product **15** in good yield, although with partial *E*/*Z* isomerization of the double bond. With respect to the alcohol scope, good to excellent yields could

be obtained for alcohols leading to stabilized radicals, such as benzylic (**16**), primary or secondary heteroatom-stabilized (**17**-**19**) or allylic (**20**-**21**).

Scheme 4. Scope for the dehydroxymethylative arylation of linear alcohols.[a]

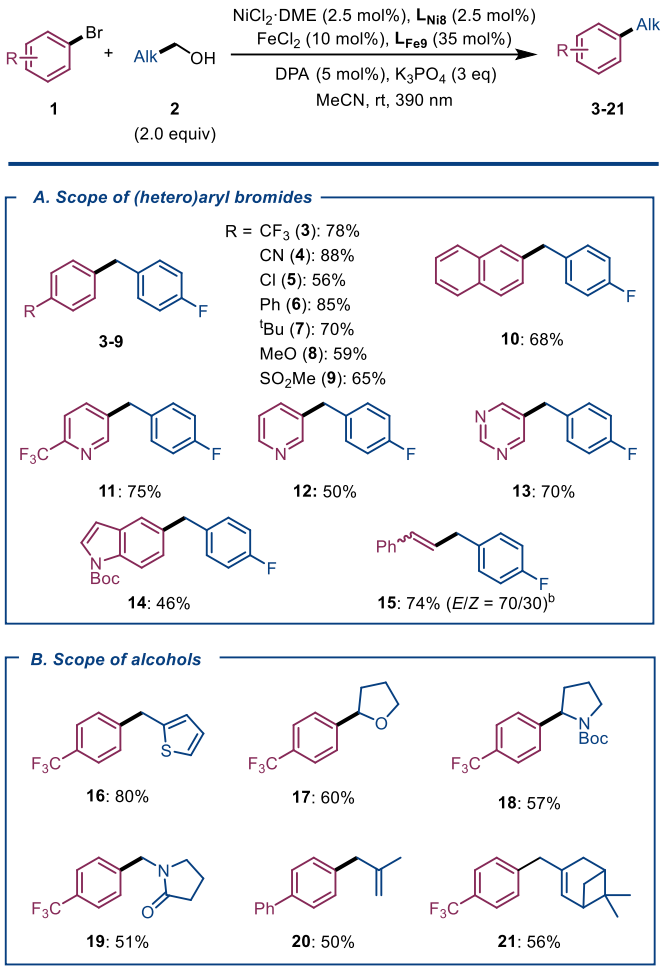

[a]Reactions performed on a 0.4 mmol scale. Isolated yields. [b]Determined by ^{1}H NMR

Having demonstrated the ability of primary alcohols to efficiently generate carbon-based radicals in this dehydroxymethylative arylation protocol, we turned our attention to more challenging sterically hindered cycloalkanols (Scheme 5A). Although C–C bond activation of this widely available substrate family would be of high interest by providing a direct entry to remotely arylated ketones, the difficulty associated with the activation of these substrates has made such transformation elusive. For these reasons, we were highly pleased to see that cycloalkanols of different ring sizes led to the corresponding ketones (**22**-**24**) in good to excellent yields. Heteroatom-containing and benzo-fuzed cycloalkanols were also suitable substrates, thus providing access to complex ketones (**25**-**26**). Similarly to the dehydroxymethylative arylation, this remote arylation protocol also featured excellent functional group compatibility, with example of electron-withdrawing and electron-donating groups, but also sensitive functionalities and nitrogen-containing heterocycles (**27**-**34**). Encouraged by this success, we wondered if *acyclic* tertiary alcohols could also be used as radical sources (Scheme 5B). Indeed, we posited that elements of both the enthalpic (*i.e.* formation of a substituted C=O bond) and the entropic drive (*i.e.* increase of conformational freedom) should be conserved between cycloalkanols and acyclic alcohols, thus making the reaction feasible on a thermodynamic ground. This transformation would be of high significance and would allow the generation of unstabilized radicals from readily available, non-toxic reagents. Although particularly challenging, a methylative cross-coupling would be exceptionally impactful due to its broad utility in bioactive molecule synthesis.[14] Additionally, despite being a very active research topic, current methylation protocols remain plagued by issues of toxicity, functional group compatibilities or atom efficiency.[15] In light of these considerations we engaged the simplest of tertiary alcohols, *tert*-butanol, in our benchmark conditions, which disappointingly led to modest yields (34%). However, the cheap, innocuous, and easy to handle α-cumyl alcohol proved to be much more efficient and the corresponding methylated products were obtained in good to average yields (**35**-**40**). Once again, the reaction was tolerant of sensitive functionalities such as a BPin group (**36**) and of biologically relevant heterocycles (**39**-**40**). Pleasingly, other *unstabilized* alkyl radicals could be generated *selectively* in this manner, as illustrated by the incorporation of cyclohexyl and *n*-butyl moieties (**41**-**43**).

Scheme 5. Scope for the arylation with tertiary alcohols.

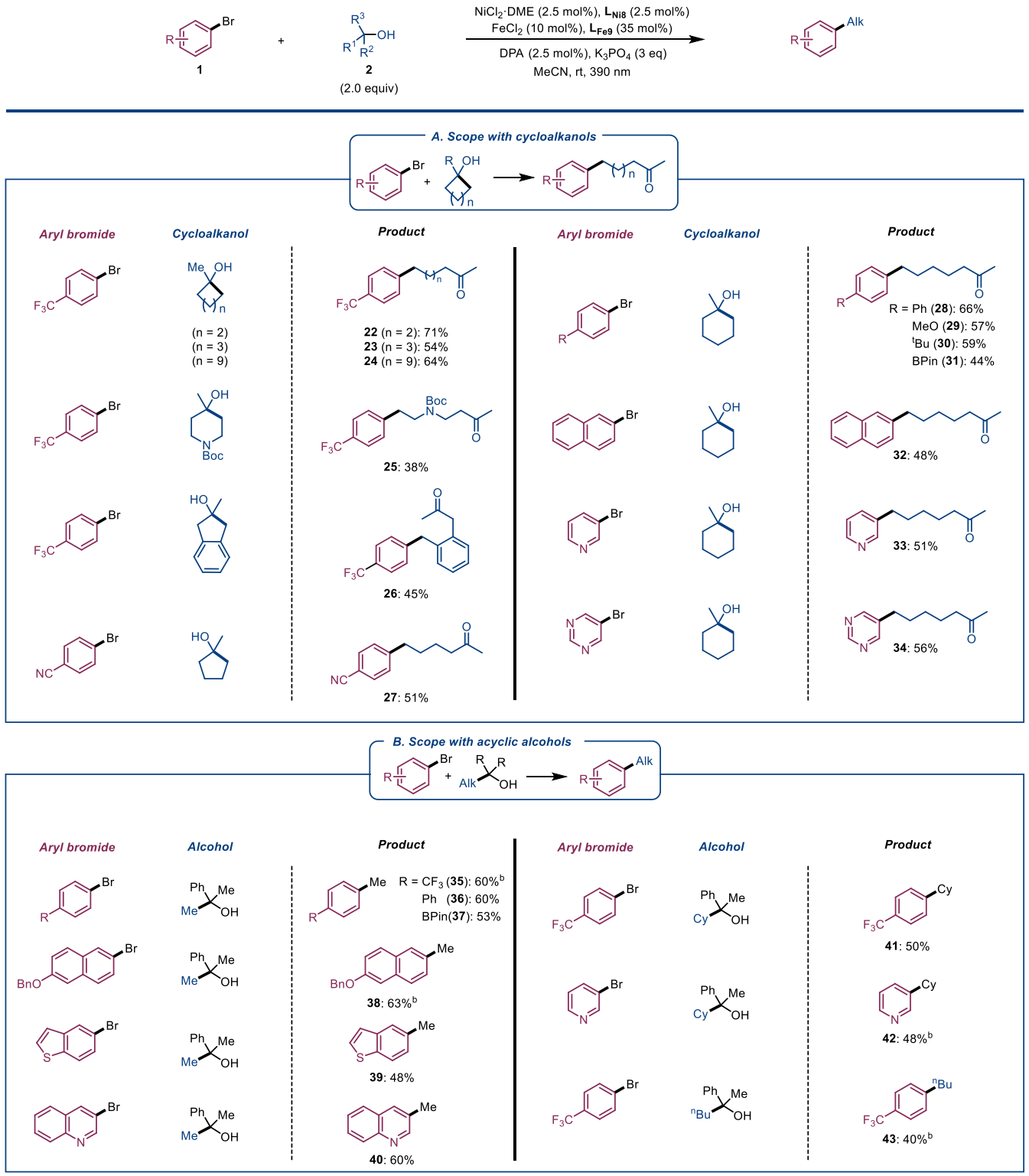

[a] Reactions performed on a 0.4 mmol scale. Isolated yields. [b] Yields determined by ^{1}H or ^{19}F NMR.

2.3. Mechanistic investigations

As previously underlined, very few dual catalyzed methods involving LMCT activation of metal-alkoxides have been described to date.[7,8] Consequently, the governing reactivity parameters and the mechanistic subtleties of this class of reactions remain essentially unknown, thus hampering its broader application to uninvestigated classes of substrates. Among the most salient questions are the

role of the iron ligand sphere and the actual involvement of iron alkoxide within the catalytic cycle. With these questions in mind, we set out to a series of cyclic voltammetry (CV) studies and stoichiometric experiments.

Firstly, we examined the cyclic voltammogram of $FeCl_2$ solutions in MeCN (0.1 M $TBAPF_6$; GC WE; Pt CE; $Ag/AgNO_3$ ref), in the absence and the presence of the carboxylate ligand $\mathbf{L_{Fe9}}$ (3.0 eq) (Figure 6A, left). Upon anodic scanning, $FeCl_2$ showed a broad quasi-reversible oxidation peak (O_1 = +0.01 V; R_1 = -0.10 V; *vs.* $Ag/AgNO_3$) corresponding to the Fe(II)/Fe(III) couple, as well as several irreversible reduction peaks at relatively high potentials (R_2 = -1.24 V; R_3 = -1.62 V). The shape of these later peaks is characteristic of electrodeposition, presumably of Fe(0) films and were associated to an intense stripping peak O_2 upon reverse oxidative scanning. Addition of 3 eq of $\mathbf{LFe_9}$ to this solution led to a marked cathodic shift of the Fe(II) to Fe(III) oxidation (O'_1 = -0.08 V) and loss of reversibility of the Fe(II)/Fe(III) couple. Indeed, the corresponding return wave R'_1 was considerably broadened and dramatically shifted to -1.08 V, suggesting an evolution of the iron coordination sphere upon oxidation. Remarkably, the newly formed species did not feature any additional reduction peaks until -2.05 V (R'_2). We then examined the effect of alcohol **2a** and K_3PO_4 on these solutions. In the case of unligated $FeCl_2$ (Figure 6A, middle), no significant change was observed on the Fe(II)/Fe(III) redox peaks O"1 and R"1. Reduction to low valent iron remains observable at relatively high potential ($R"_2$ = -1.43 V). In the case of $FeCl_2$ + $\mathbf{LFe_9}$ (Figure 6A, right), Fe(II) to Fe(III) oxidation was anodically shifted ($O'"_1$ = +0.34 V), the return wave was cathodically shifted ($R'"_1$ = -1.60 V) and the other reductive features at lower potential disappeared. Overall, these analysis highlight three beneficial consequences of $\mathbf{L_{Fe9}}$ on the [Fe] catalytic system : *i*) stabilization of the LMCT-active Fe(III) state, as evidenced by the large cathodic shift of the Fe(III) return wave R'_1; *ii*) prevention of degradation to Fe(0) particules by shifting the corresponding reductive waves outside of the DPA reduction range; *iii*) increasing interactions of [Fe] with alcohols, as suggested by the wave shifts.

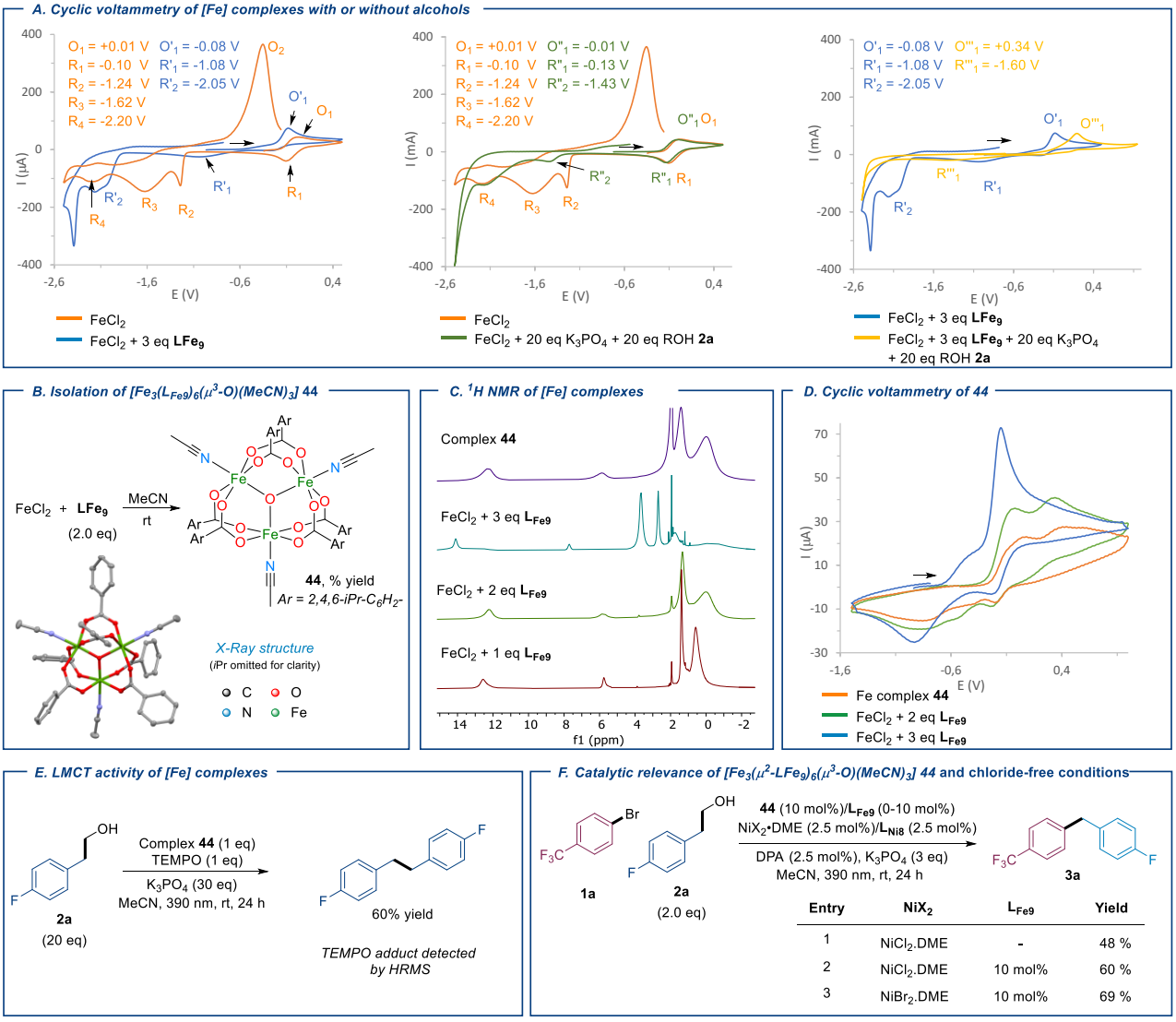

Scheme 6. Mechanistic investigations into the iron catalytic cycle. (A) Cyclic voltammetry of differently ligated $FeCl_2$; (B) Synthesis and isolation of oxo-bridged trimer **44**; (C) ^1H NMR analysis of [Fe] complexes; (D) Comparison of cyclic voltammetry of **44** and of *in-situ* formed complexes; (E) Stoichiometric LMCT activity of **44**; (F) Catalytic relevance of **44** and chloride-free conditions;

While these experiments certainly demonstrate the ability of carboxylate $\mathbf{L_{Fe9}}$ to interact with $FeCl_2$ and highlight its potential impact on catalytic efficiency, the actual nature of the corresponding species remains hazy. To shed further light on the complex identity,

$FeCl_2$ was allowed to react with various amounts of $\mathbf{L_{Fe9}}$ (1 to 3 eq) and crystallization of the corresponding complexes was attempted. While precipitation of copious amounts of chloride salts was observed in all cases, the only mixture that led to X-Ray suitable crystals was for a 1:2 $FeCl_2$:$\mathbf{L_{Fe9}}$ mixture (Scheme 6B). Strikingly, the resulting complex appeared to be the oxo-bridged trimer **44**, even though all experiments were performed in dry and degassed solvents. The Fe atoms in **44** featured two different set of bond length, characteristic of a Fe^{III}-Fe^{III}-Fe^{II} mixed-valence complex.[16] Interestingly, independent analysis of complex **44** by ^1H NMR and cyclic voltammetry showed very similar features than species formed by *in-situ* mixing of $FeCl_2$ and 2 eq of $\mathbf{L_{Fe9}}$ (Scheme 6C and 6D). However, introduction of an additional equivalent of $\mathbf{L_{Fe9}}$ led to significant spectral differences with **44**, suggesting that trimeric structures such as **44** further evolves in solution when 3 eq of $\mathbf{L_{Fe9}}$ are present. In terms of catalytic activity, complex **44** led to decreased yields compared to the benchmark conditions, but to similar yields in the presence of 10 mol% of $\mathbf{L_{Fe9}}$ (Scheme 6F, entries 1 and 2). Crucially, activation of alcohol **2a** was observed upon irradiation of complex **44** in presence of base and TEMPO, leading to good yields of the corresponding dimer and to traces of the TEMPO trapping adduct (Scheme 6E), and **44** also appeared to be catalytically active in the complete absence of chloride anions (Scheme 6F entry 3), which support the involvement of iron alkoxide as the LMCT-active species, as opposed to homolysis of a Fe-Cl bond followed by formation of a [ROH--Cl]$^\bullet$ adduct.[17]

Having clarified the behavior of the iron cycle, we went on to investigate the nickel cycle. First, we recorded the CV of ($\mathbf{LNi_8}$)$NiCl_2$ (formed *in-situ* from $NiCl_2$.DME and $\mathbf{LNi_8}$) (Scheme 7A, left). Upon cathodic scanning, two well-defined reduction waves R_1 (-1.39 V) and R_2 (-1.82 V) were observed and were respectively associated to two main return waves O_1 (-0.19 V) and O_2 (-1.12 V). Addition of aryl bromide **1a** (1 to 5 eq) led to an increased current at the second reduction peak R'_2 along with loss of the return oxidation peak O_2, while R'_1 and O'_1 remained unchanged (Scheme 7A, middle). New return oxidation waves were also observed, in particular O'_3 (-0.19 V). Persistence of O'_1 suggests that the species associated with R'_2 do not originate from R'_1 (*e.g.* Ni^{II}/Ni^{I} followed by Ni^{I}/Ni^{0}), but rather that R'_2 and R'_1 correspond to the reduction of two differently speciated Ni^{II} species.[18] Although the exact nature of these species or the number of electrons associated with R'_1 and R'_2 remain to be clarified, the magnitude of the current increase between R_2 and R_2' (from -103 μA to -260 μA) would be consistent with an initial one electron reduction from Ni^{II} to Ni^{I} followed by oxidative addition to Ni^{III} and subsequent two electrons reduction to Ni^{I}. Formation of the corresponding oxidative addition complex **45**, characterized by the return oxidation wave O'_3, was corroborated by independent synthesis (Figure 7B) and comparison of the CV analysis (Figure 7A, right). This addition complex **45** appeared to be catalytically active in standard reaction conditions (Scheme 7C).

Taken together, the above experiments support the catalytic cycle depicted in Scheme 8. First, a carboxylate-ligated Fe^{II} complex **A** (E^p_{ox} = -0.08 V) gets oxidized by DPA* ($E^{1/2}$(DPA*/DPA) = +0.95 V *vs.* Ag/$AgNO_3$)[19] to Fe^{III} complex **B**, followed by alcohol complexation.[20] The ensuing species **C** can then undergo LMCT excitation, resulting in Fe^{III}-O bond homolysis and regeneration of **A**. The nickel catalytic cycle is initiated from a Ni^{I} complex **E** that undergoes oxidative addition with ArBr to give high-valent Ni^{III} **F** which is immediately reduced to Ni^{II} **G** (E^p_{ox}(G/F) = +0.20 V) by $DPA^{-\bullet}$ ($E^{1/2}$(DPA/$DPA^{-\bullet}$) = -2.24 V).[21] Capture of radical $R^\bullet$ by **G** and reductive elimination complete the cycle.

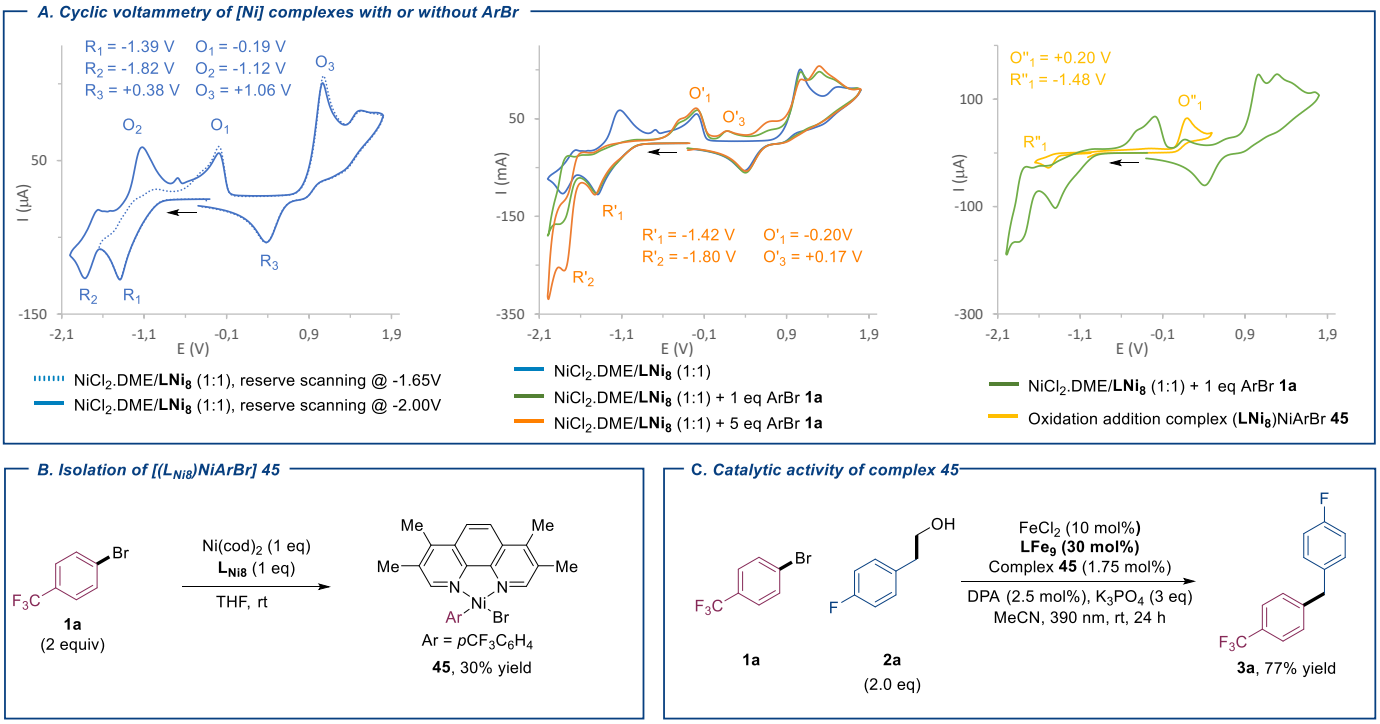

Scheme 7. Mechanistic investigations into the nickel catalytic cycle. (A) Cyclic voltammetry of $NiCl_2$•DME/$\mathbf{L_{Ni8}}$ (1:1) (left), in the presence of ArBr (middle), and comparison with isolated oxidative addition complex (right); (B) Synthesis and isolation of oxidative addition complex **45**; (C) Catalytic relevance of oxidative addition complex **45**.

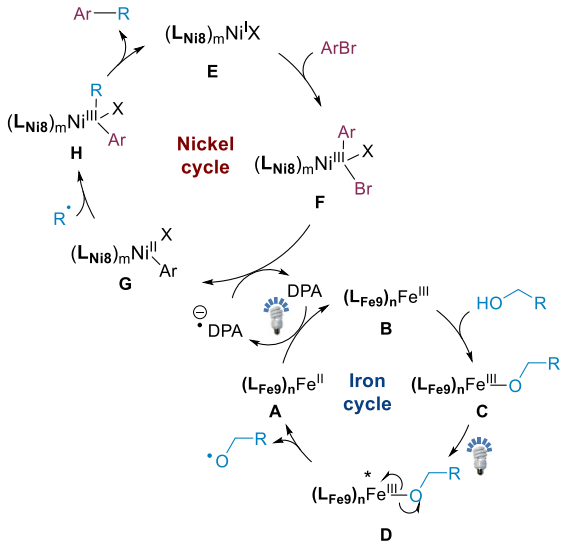

Scheme 8. Proposed catalytic pathway

3. Conclusions

In summary, we have developed a cross-coupling between a large variety of commercially available alcohols and Csp^2-halides, under mild conditions, using abundant nickel and iron catalysts. This unified strategy allows for the first time to operate *(i)* dehydroxymethylative arylation of aliphatic alcohols, *(ii)* remote arylation of cyclic alcohols to yield alkyl ketones, and *(iii)* the unprecedented use of tertiary alcohols as methyl radical source for the methylation of aryl halides.

From a broader perspective, this work demonstrates the efficient implementation of iron LMCT catalysis in the area of nickel/photoredox catalysis, thus expanding mechanistic landscape in cross-coupling reactions. This perspective is consolidated by mechanistic studies, which have shed light on some of the key features of this system. Notably, it has been demonstrated that supporting carboxylate ligands stabilize both low- and high-valent iron catalytic species toward unwanted reduction, thus favorising the desired [Fe^{III}-OR] LMCT pathway. This key insight should prove decisive in the future development of related dual catalytic systems.

Overall, this work paves the way for a large application of dual catalytic systems involving LMCT activation of alcohols, a field of tremendous potential that is promised to open vast areas of chemical space.

ASSOCIATED CONTENT

Supporting Information

The Supporting Information contains experimental procedures and graphical abstracts for the electrochemical reaction, investigation of the reaction parameters, optimization of the reaction conditions, the optimization of low yielding substrates, analysis, and compound characterization data.

AUTHOR INFORMATION

Corresponding Authors

*Abderrahmane Amgoune: abderrahmane.amgoune@univ-lyon1.fr – ORCID: 0000-0002-6195-1411
*Gaël Tran: gael.tran@univ-lyon1.fr – ORCID: 0000-0001-7817-5255

Authors

Mohammad Jaber
Yasemin Ozbay

Author Contributions

The manuscript was written through contributions of all authors. All authors have given approval to the final version of the manuscript.

ACKNOWLEDGMENT

This work was supported by the CNRS, the French Ministry of Research, the ICBMS and the Université Claude Bernard Lyon 1. The NMR and Mass Centres of the Université Claude Bernard Lyon 1 are thanked for their contribution. A. A. thanks the Institut Universitaire de France (IUF) for its support. We thank Maurice Médebielle for his help with cyclic voltammetry experiments.

REFERENCES

(1) a) Lovering, F.; Bikker, J.; Humblet, C. Escape from Flatland: Increasing Saturation as an Approach to Improving Clinical Success. *J. Med. Chem.* **2009**, *52* (21), 6752–6756. b) Lovering, F. Escape from Flatland 2: Complexity and Promiscuity. *Med. Chem. Commun.* **2013**, *4* (3), 515–519.

(2) a) Chan, A. Y.; Perry, I. B.; Bissonnette, N. B.; Buksh, B. F.; Edwards, G. A.; Frye, L. I.; Garry, O. L.; Lavagnino, M. N.; Li, B. X.; Liang, Y.; Mao, E.; Millet, A.; Oakley, J. V.; Reed, N. L.; Sakai, H. A.; Seath, C. P.; MacMillan, D. W. C. Metallaphotoredox: The Merger of Photoredox and Transition Metal Catalysis. *Chem. Rev*. **2022**, *122* (2), 1485–1542. b) Zhang, J.; Rueping, M. Metallaphotoredox Catalysis for sp^3 C–H Functionalizations through Hydrogen Atom Transfer (HAT). *Chem. Soc. Rev*. **2023**, *52* (12), 4099–4120.

(3) For selected examples, see : a) Weix, D. J. Methods and Mechanisms for Cross-Electrophile Coupling of Csp^2 Halides with Alkyl Electrophiles. *Acc. Chem. Res*. **2015**, *48* (6), 1767–1775. b) Zhang, P.; Le, C. "Chip"; MacMillan, D. W. C. Silyl Radical Activation of Alkyl Halides in Metallaphotoredox Catalysis: A Unique Pathway for Cross-Electrophile Coupling. *J. Am. Chem. Soc.* **2016**, *138* (26), 8084–8087. c) Lévêque, C.; Chenneberg, L.; Corcé, V.; Goddard, J.-P.; Ollivier, C.; Fensterbank, L. Primary Alkyl Bis-Catecholato Silicates in Dual Photoredox/Nickel Catalysis: Aryl- and Heteroaryl-Alkyl Cross Coupling Reactions. *Org. Chem. Front.* **2016**, *3* (4), 462–465. d) Jouffroy, M.; Primer, D. N.; Molander, G. A. Base-Free Photoredox/Nickel Dual-Catalytic Cross-Coupling of Ammonium Alkylsilicates. *J. Am. Chem. Soc*. **2016**, *138* (2), 475–478. e) Zuo, Z.; Ahneman, D. T.; Chu, L.; Terrett, J. A.; Doyle, A. G.; MacMillan, D. W. C. Merging Photoredox with Nickel Catalysis: Coupling of α-Carboxyl sp^3-Carbons with Aryl Halides. *Science* **2014**, *345* (6195), 437–440. f) Cornella, J.; Edwards, J. T.; Qin, T.; Kawamura, S.; Wang, J.; Pan, C.-M.; Gianatassio, R.; Schmidt, M.; Eastgate, M. D.; Baran, P. S. Practical Ni-Catalyzed Aryl–Alkyl Cross-Coupling of Secondary Redox-Active Esters. *J. Am. Chem. Soc.* **2016**, *138* (7), 2174–2177. g) Turro, R. F.; Wahlman, J. L. H.; Tong, Z. J.; Chen, X.; Yang, M.; Chen, E. P.; Hong, X.; Hadt, R. G.; Houk, K. N.; Yang, Y.-F.; Reisman, S. E. Mechanistic Investigation of Ni-Catalyzed Reductive Cross-Coupling of Alkenyl and Benzyl Electrophiles. *J. Am. Chem. Soc.* **2023**, *145* (27), 14705–14715. h) Huihui, K. M. M.; Caputo, J. A.; Melchor, Z.; Olivares, A. M.; Spiewak, A. M.; Johnson, K. A.; DiBenedetto, T. A.; Kim, S.; Ackerman, L. K. G.; Weix, D. J. Decarboxylative Cross-Electrophile Coupling of N-Hydroxyphthalimide Esters with Aryl Iodides. *J. Am. Chem. Soc.* **2016**, *138* (15), 5016–5019. i) Martin-Montero, R.; Yatham, V. R.; Yin, H.; Davies, J.; Martin, R. Ni-Catalyzed Reductive Deaminative Arylation at sp^3 Carbon Centers. *Org. Lett.* **2019**, *21* (8), 2947–2951. j) Plunkett, S.; Basch, C. H.; Santana, S. O.; Watson, M. P. Harnessing Alkylpyridinium Salts as Electrophiles in Deaminative Alkyl–Alkyl Cross-Couplings. *J. Am. Chem. Soc.* **2019**, *141* (6), 2257–2262.

(4) a) Ertl, P.; Schuhmann, T. A Systematic Cheminformatics Analysis of Functional Groups Occurring in Natural Products. *J. Nat. Prod.* **2019**, *82* (5), 1258–1263. b) Henkel, T.; Brunne, R. M.; Müller, H.; Reichel, F. Statistical Investigation into the Structural Complementarity of Natural Products and Synthetic Compounds. *Angew. Chem. Int. Ed.* **1999**, *38* (5), 643–647.

(5) For selected examples, see : a) Barton, D. H. R.; McCombie, S. W. A New Method for the Deoxygenation of Secondary Alcohols. *J. Chem. Soc., Perkin Trans. 1* **1975**, No. 16, 1574–1585. b) Lopez, R. M.; Hays, D. S.; Fu, G. C. Bu_3SnH-Catalyzed Barton−McCombie Deoxygenation of Alcohols. *J. Am. Chem. Soc.* **1997**, *119* (29), 6949–6950. c) Chenneberg, L.; Baralle, A.; Daniel, M.; Fensterbank, L.; Goddard, J.-P.; Ollivier, C. Visible Light Photocatalytic Reduction of O-Thiocarbamates: Development of a Tin-Free Barton–McCombie Deoxygenation Reaction. *Adv. Synth. Catal.* **2014**, *356* (13), 2756–2762. d) Friese, F. W.; Studer, A. Deoxygenative Borylation of Secondary and Tertiary Alcohols. *Angew. Chem. Int. Ed.* **2019**, *58* (28), 9561–9564. e) Wu, J.; Bär, R. M.; Guo, L.; Noble, A.; Aggarwal, V. K. Photoinduced Deoxygenative Borylations of Aliphatic Alcohols. *Angew. Chem. Int. Ed.* **2019**, *58* (52), 18830–18834. f) Zhang, L.; Koreeda, M. Radical Deoxygenation of Hydroxyl Groups via Phosphites. *J. Am. Chem. Soc.* **2004**, *126* (41), 13190–13191. g) Li, Z.; Sun, W.; Wang, X.; Li, L.; Zhang, Y.; Li, C. Electrochemically Enabled, Nickel-Catalyzed Dehydroxylative Cross-Coupling of Alcohols with Aryl Halides. *J. Am. Chem. Soc.* **2021**, *143* (9), 3536–3543. h) Guo, P.; Wang, K.; Jin, W.-J.; Xie, H.; Qi, L.; Liu, X.-Y.; Shu, X.-Z. Dynamic Kinetic Cross-Electrophile Arylation of Benzyl Alcohols by Nickel Catalysis. *J. Am. Chem. Soc.* **2021**, *143* (1), 513–523. i) Suga, T.; Ukaji, Y. Nickel-Catalyzed Cross-Electrophile Coupling between Benzyl Alcohols and Aryl Halides Assisted by Titanium Co-Reductant. *Org. Lett.* **2018**, *20* (24), 7846–7850. j) Jia, X.-G.; Guo, P.; Duan, J.; Shu, X.-Z. Dual Nickel and Lewis Acid Catalysis for Cross-Electrophile Coupling: The Allylation of Aryl Halides with Allylic Alcohols. *Chem. Sci.* **2018**, *9* (3), 640–645. k) Dong, Z.; MacMillan, D. W. C. Metallaphotoredox-Enabled Deoxygenative Arylation of Alcohols. *Nature* **2021**, *598* (7881), 451–456. l) Cong, F.; Lv, X.-Y.; Day, C. S.; Martin, R. Dual Catalytic Strategy for Forging sp^2–sp^3 and sp^3–sp^3 Architectures via β-Scission of Aliphatic Alcohol Derivatives. *J. Am. Chem. Soc.* **2020**, *142* (49), 20594–20599.

(6) Tsui, E.; Wang, H.; Knowles, R. R. Catalytic Generation of Alkoxy Radicals from Unfunctionalized Alcohols. *Chem. Sci.* **2020**, *11* (41), 11124–11141.

(7) Huang, L.; Ji, T.; Rueping, M. Remote Nickel-Catalyzed Cross-Coupling Arylation via Proton-Coupled Electron Transfer-Enabled C–C Bond Cleavage. *J. Am. Chem. Soc*. **2020**.

(8) Chen, Y.; Wang, X.; He, X.; An, Q.; Zuo, Z. Photocatalytic Dehydroxymethylative Arylation by Synergistic Cerium and Nickel Catalysis. *J. Am. Chem. Soc.* **2021**, *143* (13), 4896–4902.

(9) a) May, A. M.; Dempsey, J. L. A New Era of LMCT: Leveraging Ligand-to-Metal Charge Transfer Excited States for Photochemical Reactions. *Chem. Sci.* **2024**, *15* (18), 6661–6678. b) Juliá, F. Ligand-to-Metal Charge Transfer (LMCT) Photochemistry at 3d-Metal Complexes: An Emerging Tool for Sustainable Organic Synthesis. *ChemCatChem* **2022**, *14* (19), e202200916.

(10) Abderrazak, Y.; Bhattacharyya, A.; Reiser, O. Visible-Light-Induced Homolysis of Earth-Abundant Metal-Substrate Complexes: A Complementary Activation Strategy in Photoredox Catalysis. *Angew. Chem. Int. Ed.* **2021**, *60* (39), 21100–21115.

(11) For reported examples of alcohols activation involving Fe LMCT, see a) Reichgott, D. W.; Rose, N. J. Photoassisted Oxidation of Methanol Catalyzed by a Macrocyclic Iron Complex. *J. Am. Chem. Soc.* **1977**, *99* (6), 1813–1818. b) Liu, W.; Wu, Q.; Wang, M.; Huang, Y.; Hu, P. Iron-Catalyzed C–C Single-Bond Cleavage of Alcohols. *Org. Lett.* **2021**, *23* (21), 8413–8418. c) Xiong, N.; Li, Y.; Zeng, R. Iron-Catalyzed Photoinduced Remote C(Sp3)–H Amination of Free Alcohols. *Org. Lett.* **2021**, *23* (22), 8968–8972. d) Xue, T.; Zhang, Z.; Zeng, R. Photoinduced Ligand-to-Metal Charge Transfer (LMCT) of Fe Alkoxide Enabled C–C Bond Cleavage and Amination of Unstrained Cyclic Alcohols. *Org. Lett.* **2022**, *24* (3), 977–982.

(12) For rare examples of arylations by dual catalysis involving Fe LMCT, see: a) Zou, L.; Wang, X.; Xiang, S.; Zheng, W.; Lu, Q. Paired Oxidative and Reductive Catalysis: Breaking the Potential Barrier of Electrochemical C(sp^3)−H Alkenylation. *Angew. Chem. Int. Ed.* **2023**, *62* (24), e202301026. b) Xiong, N.; Li, Y.; Zeng, R. Merging Photoinduced Iron-Catalyzed Decarboxylation with Copper Catalysis for C–N and C–C Couplings. *ACS Catal.* **2023**, *13* (3), 1678–1685. c) Zou, L.; Xiang, S.; Sun, R.; Lu, Q. Selective C(sp^3)–H Arylation/Alkylation of Alkanes Enabled by Paired Electrocatalysis. *Nat Commun* **2023**, *14* (1), 7992.

(13) a) de Groot, L. H. M.; Ilic, A.; Schwarz, J.; Wärnmark, K. Iron Photoredox Catalysis–Past, Present, and Future. *J. Am. Chem. Soc.* **2023**, *145* (17), 9369–9388. b) Chen, J.; Browne, W. R. Photochemistry of Iron Complexes. *Coordination Chemistry Reviews* **2018**, *374*, 15–35. c) Zhou, W.-J.; Wu, X.-D.; Miao, M.; Wang, Z.-H.; Chen, L.; Shan, S.-Y.; Cao, G.-M.; Yu, D.-G. Light Runs Across Iron Catalysts in Organic Transformations. *Chemistry – A European Journal* **2020**, *26* (66), 15052–15064.

(14) Barreiro, E. J.; Kümmerle, A. E.; Fraga, C. A. M. The Methylation Effect in Medicinal Chemistry. *Chem. Rev.* **2011**, *111* (9), 5215–5246.

(15) For selected examples, see : a) Huihui, K. M. M.; Caputo, J. A.; Melchor, Z.; Olivares, A. M.; Spiewak, A. M.; Johnson, K. A.; DiBenedetto, T. A.; Kim, S.; Ackerman, L. K. G.; Weix, D. J. Decarboxylative Cross-Electrophile Coupling of N-Hydroxyphthalimide Esters with Aryl Iodides. *J. Am. Chem. Soc*. **2016**, *138* (15), 5016–5019. b) Zhang, P.; Le, C. "Chip"; MacMillan, D. W. C. Silyl Radical Activation of Alkyl Halides in Metallaphotoredox Catalysis: A Unique Pathway for Cross-Electrophile Coupling. *J. Am. Chem. Soc.* **2016**, *138* (26), 8084–

8087. c) Kariofillis, S. K.; Shields, B. J.; Tekle-Smith, M. A.; Zacuto, M. J.; Doyle, A. G. Nickel/Photoredox-Catalyzed Methylation of (Hetero)Aryl Chlorides Using Trimethyl Orthoformate as a Methyl Radical Source. *J. Am. Chem. Soc.* **2020**, *142* (16), 7683–7689. d) Jin, J.; MacMillan, D. W. C. Alcohols as Alkylating Agents in Heteroarene C–H Functionalization. *Nature* **2015**, *525* (7567), 87–90. e) Chen, R.; Intermaggio, N. E.; Xie, J.; Rossi-Ashton, J. A.; Gould, C. A.; Martin, R. T.; Alcázar, J.; MacMillan, D. W. C. Alcohol-Alcohol Cross-Coupling Enabled by SH2 Radical Sorting. *Science* **2024**, *383* (6689), 1350–1357. f) He, Z.-T.; Li, H.; Haydl, A. M.; Whiteker, G. T.; Hartwig, J. F. Trimethylphosphate as a Methylating Agent for Cross Coupling: A Slow-Release Mechanism for the Methylation of Arylboronic Esters. *J. Am. Chem. Soc.* **2018**, *140* (49), 17197–17202. g) Heijnen, D.; Tosi, F.; Vila, C.; Stuart, M. C. A.; Elsinga, P. H.; Szymanski, W.; Feringa, B. L. Oxygen Activated, Palladium Nanoparticle Catalyzed, Ultrafast Cross-Coupling of Organolithium Reagents. *Angew. Chem. Int. Ed.* **2017**, *56* (12), 3354–3359.

(16) a) Cannon, R. D.; Montri, L.; Brown, D. B.; Marshall, K. M.; Elliott, C. M. Partial Electron Delocalization in a Mixed-Valence Trinuclear Iron(III)-Iron(II) Complex. *J. Am. Chem. Soc.* **1984**, *106* (9), 2591–2594. b) Overgaard, J.; Larsen, F. K.; Schiøtt, B.; Iversen, B. B. Electron Density Distributions of Redox Active Mixed Valence Carboxylate Bridged Trinuclear Iron Complexes. *J. Am. Chem. Soc.* **2003**, *125* (36), 11088–11099.

(17) a) An, Q.; Xing, Y.-Y.; Pu, R.; Jia, M.; Chen, Y.; Hu, A.; Zhang, S.-Q.; Yu, N.; Du, J.; Zhang, Y.; Chen, J.; Liu, W.; Hong, X.; Zuo, Z. Identification of Alkoxy Radicals as Hydrogen Atom Transfer Agents in Ce-Catalyzed C–H Functionalization. *J. Am. Chem. Soc.* **2023**, *145* (1), 359–376. b) Yang, Q.; Wang, Y.-H.; Qiao, Y.; Gau, M.; Carroll, P. J.; Walsh, P. J.; Schelter, E. J. Photocatalytic C–H Activation and the Subtle Role of Chlorine Radical Complexation in Reactivity. *Science* **2021**, *372* (6544), 847–852.

(18) a) Chrisman, C. H.; Kudisch, M.; Puffer, K. O.; Stewart, T. K.; Lamb, Y. M. L.; Lim, C.-H.; Escobar, R.; Thordarson, P.; Johannes, J. W.; Miyake, G. M. Halide Noninnocence and Direct Photoreduction of Ni(II) Enables Coupling of Aryl Chlorides in Dual Catalytic, Carbon–Heteroatom Bond-Forming Reactions. *J. Am. Chem. Soc.* **2023**, *145* (22), 12293–12304. (b) Vander Griend, D. A.; Bediako, D. K.; DeVries, M. J.; DeJong, N. A.; Heeringa, L. P. Detailed Spectroscopic, Thermodynamic, and Kinetic Characterization of Nickel(II) Complexes with 2,2'-Bipyridine and 1,10-Phenanthroline Attained via Equilibrium-Restricted Factor Analysis. *Inorg. Chem.* **2008**, *47* (2), 656–662.

(19) Neumeier, M.; Chakraborty, U.; Schaarschmidt, D.; de la Pena O'Shea, V.; Perez-Ruiz, R.; Jacobi von Wangelin, A. Combined Photoredox and Iron Catalysis for the Cyclotrimerization of Alkynes. *Angew. Chem. Int. Ed.* **2020**, *59* (32), 13473–13478.

(20) At this stage, we cannot exclude complexation of [Fe^{II}] by ROH first, followed by oxidation to [Fe^{III}-OR]

(21) Comproportionation with remaining Ni^{I} **E** is also possible. Reduction of the resulting ($\mathbf{L_{Ni8}}$)m$Ni^{II}X_2$ complex by $DPA^{-\bullet}$ would then turn over the cycle.